THE PRINCIPLE OF ADAPTIVE EXCITATION FOR PHOTOLUMINESCENCE IMAGING OF SILICON: THEORY

Friedemann D. Heinz[1,3*], Yan Zhu[2], Ziv Hameri[2], Mattias Juhl[2], Thorsten Trupke[2], Martin C. Schubert[1]

[1]Fraunhofer ISE, Heidenhofstr. 2, 79110 Freiburg, Germany

[2]The University of New South Wales, Sydney, Australia

[3]University of Freiburg, Germany

[*]friedemann.heinz@ise.fraunhofer.de

Abstract An approach that determines the charge carrier lifetime from photoluminescence (PL) imaging that is virtually not affected by lateral charge carrier drift and diffusion and image smearing due to photon scattering is proposed. The approach attempts to create a laterally uniform charge carrier density within a sample with non-homogeneous recombination properties via illumination with spatially varying intensity. Lateral excess charge carrier drift and diffusion is inherently absent in this situation. Furthermore, as a homogeneous PL intensity is monitored, any optical artefact induced by photon scattering in the investigated wafer or the detection charge-coupled device is strongly suppressed compared to conventional PL imaging. Using numeric simulations of different lifetime distribution scenarios, including one based on measured micro-Photoluminescence (μ-PL) lifetime data, we demonstrate the feasibility of this proposed "Adaptive Excitation Photoluminescence Imaging" (Ax-PLI) method.

1 Introduction

In the past decade photoluminescence imaging [1] (PLI) gained prominence for spatially resolved characterisation of silicon wafers and solar cells with non-uniform recombination

properties [1]. The spatial resolution of the PL image is commonly defined as the sample area corresponding to a single pixel of a charge-coupled device (CCD), typically a square of about 100 micrometres edge length. However, there are several factors which lead to a strong decrease of the obtained effective resolution.

The major effects are: scattering of PL (1) within the silicon (Si) CCD chip used for detection and (2) within the wafer. Both effects primarily affect the long wavelength components of the PL spectrum. An approach to address (1) is post-processing of the PL image by means of measurement system specific deconvolution [2,3]. While the system dependence (lenses, filters etc.) can be dealt with, the emission spectrum of the specific sample also has to be taken into account; e.g. the reabsorption of PL in a thick sample determines the spectral composition of the PL. Scattering of the PL in the sample (2) means that long wavelength photons may traverse laterally within the wafer and emerge from the wafer at a distant location.

Another difficulty of quantitative lifetime measurement metrology on non-uniform material is the bulk diffusion length of the excess charge carriers, in particular in state-of-the-art material of high quality such as high performance multicrystalline silicon [4]. Any spatially confined defect of high recombination activity embedded in a material of high diffusion length inevitably depletes adjacent regions from excess charge carriers (with density δn). The resulting excess charge carrier gradients under steady state conditions are reflected directly in the PL image. In order to account for diffusion when using PLI, it was proposed to apply de-smearing [5,6] by explicit calculation of the diffusion term $\sim \mathrm{grad}\, \delta n$ in the continuity equation (see below) from the measured δn image. Experimentally this approach is limited to devices without a junction, as it cannot account for drift, and by the introduction of strong noise by the Laplacian operation. In addition to the above complications for (1) and (2), there is a condition which is practically never

accounted for within the concept of de-smearing except when measuring at very low intensities: the injection independence of the minority charge carrier lifetime.

Generally, this injection dependence creates a limitation for PLI-based basic physics investigations. PLI is conducted at a laterally constant generation rate g across the sample. Be the absorption depth comparable or larger than the wafer thickness, we then may write the continuity equation for the excess charge carrier density in steady state:

$$g + \mathrm{div}\left\{D\left(\delta n^{(x,y)}\right)\mathrm{grad}\ \delta n^{(x,y)}\right\} = \frac{\delta n^{(x,y)}}{\tau^{(x,y)}\left(\delta n^{(x,y)}\right)} \quad (1)$$

with the recombination lifetime $\tau = \tau^{(x,y)}\left(\delta n^{(x,y)}\right)$ depending on the position (x,y), and with the diffusion coefficient D. Measurements at a constant generation rate lead to laterally inhomogeneous "injection" ($\delta n^{(x,y)}$ in steady state) and a driving force for lateral drift and diffusion. Uniform illumination reflects a device's operation condition, thus PLI can be used as a fast and sensitive metric for solar cell technological assessment. However, when using PLI for a quantitative charge carrier lifetime analysis, caution has to be taken, precisely because the lifetime is a function of the local injection.

We propose an approach based on excitation with laterally *non*-uniform intensity which has the potential of being virtually free from any of the carrier smearing and photon scattering related deficiencies of PLI discussed above; we named this method as adaptive-excitation PLI (Ax-PLI). Non-uniform excitation patterns with a high spatial resolution can be obtained using light sources in combination with e.g. digital micro mirror device (DMD), which has been used to determine sheet resistance and diffusion length in solar cells [7], or liquid crystal devices (LCD), which is discussed in section 4. In the following we state the principle motivation for – and the implications of laterally non-uniform excitation. We propose an iterative procedure suitable for an experimental realisation, and verify the validity of the proposed method using numeric

simulations. The influence of finite penetration depth of the excitation light and photon smearing is considered and a practical example based on experimental lifetime data is presented.

2 Approach

The steady state continuity equation of excess charge carriers, Eq. 1, suggests one way to proceed in order to suppress net lateral charge carrier movement: if the spatial excess minority charge carrier density profile is laterally constant, then there is no driving force for lateral diffusion or drift. We choose a generation rate $g_{\infty}^{(x,y)}$ such that $\mathrm{grad}\left(\delta n^{(x,y)}\right) = 0$ (and $\delta n^{(x,y)} = \mathrm{const.} =: \delta n_{\infty}$), in other words, a generation rate that results in a spatially constant excess charge carrier density. The choice of "∞" as subscript becomes clear later. In this case, Eq. 1 reduces to

$$g_{\infty}^{(x,y)} = \frac{\delta n_{\infty}}{\tau^{(x,y)}(\delta n_{\infty})} \qquad (2)$$

If such a generation rate $g_{\infty}^{(x,y)}$ can be found, the charge carrier lifetime $\tau^{(x,y)}$ may be inferred directly from the generation rate $g_{\infty}^{(x,y)}$ itself by inversion of Eq. 2. Lateral diffusion and drift are absent. Furthermore, photon scattering is only a problem for PL images which show a high intensity contrast. Since $I_{\mathrm{pl}}^{(x,y)} = \mathrm{const.}$ for Ax-PLI, i.e. vanishing image contrast, the effect of photon scattering is significantly reduced for the proposed technique.

We now discuss an approach to *experimentally* find a suitable non-uniform generation rate $g_{\infty}^{(x,y)}$ which causes a constant excess charge carrier density. In the absence of information about the lateral lifetime distribution in a specific sample, the starting point is a PLI measurement with laterally uniform generation rate g_0, the subscript "0" denoting the starting condition of an iterative procedure to determine the generation profile $g_{\infty}^{(x,y)}$ that results in the desired uniform charge carrier density δn_{∞}. The proposed adaptive procedure for finding $g_{\infty}^{(x,y)}$ is intuitive: illuminating regions of high recombination activity (i.e. lower charge carrier density in steady

state) with higher excitation intensity. The excitation intensity $g_{\infty}^{(x,y)}$ required to generate a particular uniform injection level δn_{∞} (the "target" injection level) is $g_{\infty}^{(x,y)} = \delta n_{\infty}/\tau^{(x,y)}$ where $\tau^{(x,y)}$ is the actual charge carrier lifetime. As $\tau^{(x,y)}$ is a priori unknown, we define an iterative procedure

$$g_{k+1}^{(x,y)} = \varepsilon \frac{\delta n_{\infty}}{\tau_k^{(x,y)}\left(\delta n_k^{(x,y)}\right)} + (1-\varepsilon) g_k^{(x,y)}$$

$$= g_k^{(x,y)} \left\{ \varepsilon \left(\frac{\delta n_{\infty}}{\delta n_k^{(x,y)}} - 1 \right) + 1 \right\} \quad (3)$$

with $\tau_0^{(x,y)} = \delta n_0^{(x,y)}/g_0 = \tau_{\text{eff}}^{(x,y)}$ where g_0 is a uniform generation rate. In Eq.3 we introduced a damping parameter $0 < \varepsilon < 1$ which ensures convergence: Due to the injection dependence of the charge carrier lifetime a fast change of the charge carrier density in one iteration step can lead to a strong change of the lifetime and the occurring oscillations may impede convergence. In this publication, the rate of convergence is not considered important, and so low epsilon values have been used to ensure that convergence is achieved. For discrete pixels (x_i, y_j) we define

$$\frac{g_{\mathrm{k}+1} - g_k}{g_k} = \frac{1}{NM} \sqrt{\sum_{j=1}^{M} \sum_{i=1}^{N} \left(\frac{g_{\mathrm{k}+1}^{(x_i,y_j)} - g_{\mathrm{k}}^{(x_i,y_j)}}{g_{\mathrm{k}}^{(x_i,y_j)}} \right)^2} \quad (4)$$

where N and M are the numbers of equidistant pixels in x and y direction. This term represents the average change in generation across the entire sample. If $\lim_{k\to\infty} (g_{k+1} - g_k)/g_k = 0$, we obtain $\lim_{k\to\infty} \left(g_{\mathrm{k}+1}^{(x_i,y_j)} - g_{\mathrm{k}}^{(x_i,y_j)} \right)/g_{\mathrm{k}}^{(x_i,y_j)} = 0$ and thus $\delta n_{\infty} = n_k^{(x,y)}$ for any ε and any (x_i, y_j). The latter implies $\nabla \delta n^{(x,y)} = 0$, as desired. Thus, if the condition $\lim_{k\to\infty} (g_{k+1} - g_k)/g_k = 0$, which can be monitored *experimentally*, is established after a certain number of iterations, $n_k^{(x,y)} = \delta n_{\infty}$ is uniform, $g_{\infty}^{(x,y)}$ is found and the charge carrier lifetime $\tau^{(x,y)}(\delta n_{\infty}) =$

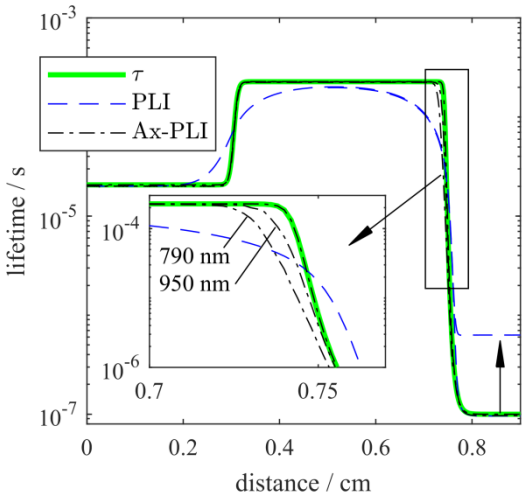

Figure 1: Lifetime distribution in a hypothetical sample, which has three distinct lifetime regions. The green solid line shows the assumed lifetime. The dashed and the dashed-dotted lines show the lifetime as measured with PLI and Ax-PLI, respectively. In the inset the influence of a finite excitation wavelength on Ax-PLI is shown (negligible influence on PLI).

$\delta n_\infty / g_\infty^{(x,y)}$ for the chosen charge carrier density δn_∞ can be inferred. In the following section the convergence of the procedure is demonstrated for typical situations by means of numeric simulations.

3 Convergence and Accuracy

In order to demonstrate the convergence and the potential of the described approach we perform numerical simulations of the adaptive procedure by means of a sample with three regions of different charge carrier lifetime for scenarios with increasing complexity: Scenario 1 assumes low injection, scenario 2 assumes higher injection where lifetime, limited by Shockley-Read-Hall recombination [8] through iron boron pairs, becomes strongly injection dependent, scenario 3 deals with finite excitation penetration depth and scenario 4 includes photon scattering. The 2D numerical simulation (simulation along a line of 9 mm length and sample depth) is implemented in Matlab. We conclude with simulations based on experimental lifetime data obtained from µ-PL measurements. Details on the used state of the art models within the simulation are given elsewhere [9].

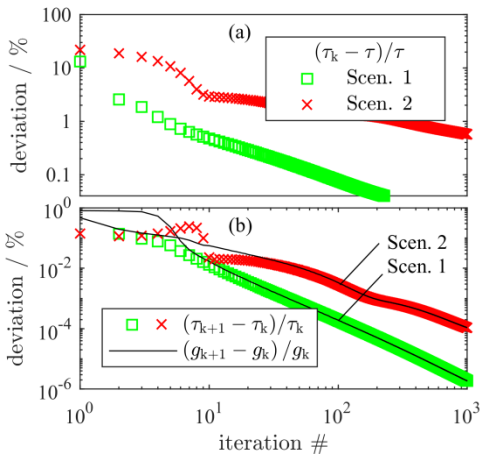

Figure 2: Convergence of the lifetime (a) and of the iteration steps (b) for both scenarios (see text for details).

The simulated sample is 200 µm thick, p-type, 1 Ωcm, with negligible surface recombination. The sample is divided into three regions of different charge carrier lifetime. The lifetime distribution is given by recombination via interstitial iron (Fe) in the left and middle regions ($[Fe_i] = 10^{11}$ and 10^{10} cm^{-3}, respectively) [8] and by constant lifetime of 100 ns on the right side, representing a localised area of high recombination activity. The lifetime between the transitions were slightly smeared to avoid singularities in the simulations. This leads to the lifetime depicted in Figure 1 (solid green curve) for an injection level of $\delta n_\infty = 10^{10}$ cm^{-3}. The blue dashed line in Figure 1 presents the lifetime as it would be measured with PLI.

First, we investigate in scenario 1 a low injection measurement with $\delta n_\infty = 10^{10}$ cm^{-3} and homogeneous excitation with sample depth. The dashed-dotted line in Figure 1 coinciding with the green solid line (cf. inset) indicates the lifetime as simulated using the Ax-PLI approach proposed here. Figure 1 demonstrates that this approach retrieves the actual charge carrier lifetime, in contrast to PLI (blue, dashed line), which is affected by lateral diffusion. Note there was not drift in the simulated sample as it has no diffused surface layers or metal contacts. In scenario 2 the simulations were repeated for a higher injection level of $\delta n_\infty = 10^{15}$ cm^{-3}. The actual charge carrier lifetime is retrieved in this scenario, too (not shown), however requiring more iterative steps as discussed in the following.

Figure 2a shows the convergence of the lifetime measured with Ax-PLI towards the actual charge carrier lifetime τ for scenario 1 and 2. The incremental change $(\tau_{k+1} - \tau_k)/\tau_k$ and the deviation $(\tau_k - \tau)/\tau$ are calculated similar to Eq. 4. For scenario 1 $(\tau_k - \tau)/\tau < 1\%$ is obtained after 5 iterations and for scenario 2 after 300 iterations (a lower damping constant $\varepsilon = 0.15$ had to be chosen in scenario 2 to suppress oscillations which in the present case hinder convergence). Furthermore, the change in generation rate $(g_{k+1} - g_k)/g_k$ converges towards zero (Figure 2b), from Eq. 3 follows that the charge carrier density $n_k^{(x,y)}$ at every pixel (x, y) converges to δn_∞. As expected from Eq. 2, $(\tau_{k+1} - \tau_k)/\tau_k$ becomes identical to $(g_{k+1} - g_k)/g_k$ after several iterations when diffusion is vanishing (cf. Figure 2b) and $\tau^{(x,y)} = \delta n^{(x,y)}/g^{(x,y)} = \delta n_\infty/g^{(x,y)}$ and thus $(\tau_{k+1} - \tau_k)/\tau_k = (g_{k+1} - g_k)/g_k$.

In the next step (scenario 3) we investigate the influence of a finite absorption depth of the excitation light. We repeat the simulation with $\delta n_\infty = 10^{10}$ cm^{-3}, using excitation wavelengths of 790 nm and 950 nm, which covers the range of wavelengths typically used in PL imaging. The excess charge carrier density was calculated taking into account non-uniform charge carrier densities with depth [9]. We find that only at the steep slope between area 2 and 3 the lifetime determined with Ax-PLI shows slight deviations from the actual lifetime as can be seen in the inset of Figure 1. The low lifetime region cannot obtain a uniform charge carrier density with depth and thus charge carriers diffuse from the high lifetime regions into the low lifetime region near the back surface where there is lower charge carrier generation. Clearly, for 950 nm excitation the deviation is less than for 790 nm excitation. Compared to the deviation of PLI lifetime from the actual charge carrier lifetime these deviations are small.

In scenario 4 we repeat the simulation with 950 nm excitation and add photon scattering: 1% of the PL emitted from each pixel on the sample is redistributed evenly among all other pixels (i.e. a point spread function with infinite extension which yields the worst case). For PLI this

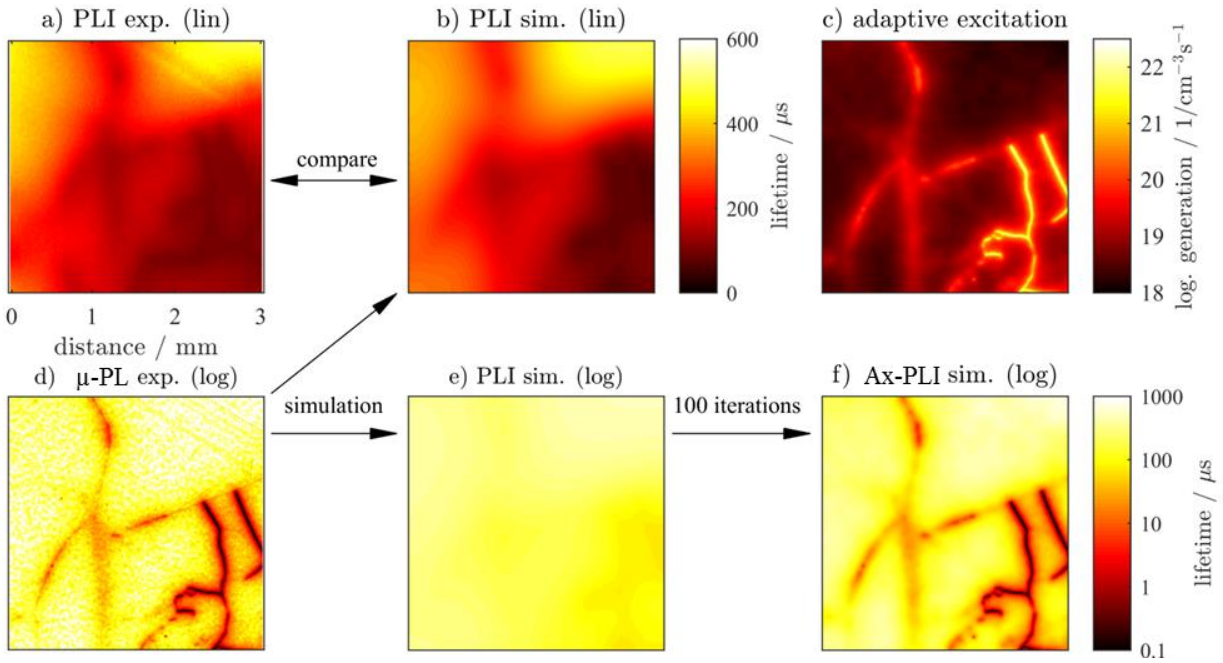

Figure 3(a) and (d) show the charge carrier lifetime measured experimentally on a multicrystalline silicon sample (see text for details) with PLI and µ-PL, respectively. From the data in (d), assumed to represent the bulk lifetime, the PLI lifetime measurement is simulated and plotted linearly in (b) and logarithmically in (e). The proposed Ax-PLI recovers the lifetime distribution with high resolution (f) by finding the excitation pattern (c) which generates uniform injection. Figures (a) and (b) are scaled identically; Figures (d) – (f) are scaled identically.

leads to a strong increase of the measured lifetime in area 3 (cf. right vertical arrow in Figure 1). As expected we do not observe an influence on Ax-PLI (i.e. the result is identical to scenario 3 with 950 nm).

Finally, the relevance of Ax-PLI is underlined using experimental lifetime data. In [10] the authors discussed a direct comparison between experimental µ-PL and PLI data from a multi-crystalline Si sample. We recall the main conclusions: (1) PLI is limited by lateral diffusion which is challenging to correct, (2) µ-PL is virtually not affected by lateral diffusion owing to material inhomogeneities, and the strong lateral diffusion due to using a point source illumination can almost completely be corrected for and (3) simulation of a PLI measurement (Figure 3b and e with linear and logarithmic scaling, respectively) using the lifetime measured with µ-PL (Figure 3d) shows excellent agreement with the PLI lifetime measurement (Figure 3a). The simulated PLI lifetime (with photon scattering) in Figure 3b corresponds quantitatively to the experimental PLI lifetime image in Figure 3a. In the following we investigate whether we can recover the µ-PL

lifetime – which we may take as a representative of a realistic lifetime distribution in a state of the art silicon sample as shown in [10] – from the PLI data simulated with this µ-PL lifetime distribution. An injection independent lifetime caused by iron boron pairs was assumed.

The region of interest of the multi-crystalline sample is 3×3 mm²×150 µm. The sample is *n*-type with a doping density of 5.8×10^{15} cm^{-3}, with no diffused layers and is surface-passivated employing an Al_2O_3 layer. The sample lifetime determined with µ-PL spans from 100 ns to 1 ms (Figure 3d). The µ-PL data was recorded with 700×700 px² at an injection level comparable to PLI. For a direct comparison to µ-PL we assume the excitation and detection resolution of Ax-PLI to be 700×700 px², too. We assume a homogeneous excitation of charge carriers with sample depth. After 100 iterations (Figure 3f) the µ-PL lifetime (Figure 3d) is retrieved, demonstrating that Ax-PLI is able to provide the actual charge carrier lifetime when using long wavelength excitation light.

4 Uncertainties expected in experiment.

From Eq. 2 it follows that an uncertainty s_g in the generation rate g leads to an error $s_\tau = \delta n/g^2\, s_g$ in the lifetime, with linear correlation, i.e. the relative error $s_\tau/\tau = s_g/g$ translates directly to the deduced lifetime. However, owing to the higher photon flux and the shorter wavelength of the excitation light compared to the PL emission, the statistical error s_g is negligible compared to the error in the PL intensity measurement s_{pl}.

In the elaborated scenarios about 10 iterations were necessary to obtain a deviation below 1% of the injection level from the targeted level; for the special case of strong injection dependence of the minority charge carrier lifetime (and high damping) up to 300 iterations are required. It has to be kept in mind that this states an *upper limit* for an investigation of a Si sample contaminated with a defect which induces a highly injection dependent charge carrier lifetime, and with a slow but robust convergence algorithm. Furthermore, more sophisticated iterative procedures and de-

smearing steps may substantially speed up the procedure. A detailed analysis of the ideal iterative procedure depends on the individual experimental realisation and the corresponding experimental noise. This work shows the principal feasibility of adaptive excitation for more accurate PL based minority carrier lifetime imaging.

In an experiment, the quality of the excitation pattern, i.e. the contrast ratio between closely spaced pixels, will be limiting the accuracy. A straight forward approach could combine a commercial LCD with monochromatic steady state laser illumination. At present LCD projectors typically achieve contrast ratios beyond 50.000:1, meaning that a sample with a charge carrier lifetime variation over 4 orders (cf. Figure 3d) of magnitude could be measured with Ax-PLI. In practice, the contrast ratio would have to be investigated in detail to show its validity towards small scales (i.e. for adjacent or closely spaced pixels). Yet, it has to be kept in mind that the spatial resolution (number of pixels) of currently available LCDs strongly exceed the resolution of scientific CCD cameras with notable quantum efficiency beyond 950 nm suitable for detection of the PL of silicon. Furthermore, due to the shorter wavelength of the excitation light compared to PL, the photon smearing in an LCD may be significantly lower than the photon smearing of long wavelength photons in the silicon CCD used in conventional PL imaging. An additional problem occurs with DMDs operating with light pulses. Being far away from steady state conditions the use of a DMD will lead to problems when dealing with injection dependent lifetimes.

5 Conclusions

In this contribution a novel PL imaging technique with adaptive illumination pattern is proposed. With this approach artefacts from charge carrier drift and diffusion and image blurring can be effectively avoided. It is shown by numeric simulations how the right choice of non-uniform illumination generates a constant charge carrier density. We propose an iterative

procedure and demonstrate a good convergence also for scenarios which show a strong injection dependence of the lifetime. The influence of finite penetration depths is investigated and a simulation using experimental lifetime data measured with micro PL mapping confirms the potential of this approach. We expect that this method will open a new field for the quantitative investigation of non-uniform material like high performance mc silicon.

Acknowledgements

This work was funded by the projects LIMES by the German Federal Ministry of Economic Affairs and Energy and CCPV by the German Federal Ministry of Research and Education. The authors also acknowledge support from the Australian Government through the Australian Renewable Energy Agency (ARENA, Project 2014/RND097) and the Australian Research Council (ARC, Project DE150100268). The views expressed herein are not necessarily the views of the Australian Government, and the Australian Government does not accept responsibility for any information or advice contained herein.

References

[1] T. Trupke, R. A. Bardos, M. C. Schubert, and W. Warta, Applied Physics Letters **89**, 44107 (2006).

[2] O. Breitenstein, F. Fruhauf, and A. Teal, IEEE J. Photovoltaics **6**, 522 (2016).

[3] D. Walter *et al.*, IEEE J. Photovoltaics **4**, 368 (2014).

[4] F. Schindler *et al.*, Solar Energy Materials and Solar Cells **171**, 180 (2017).

[5] S. P. Phang, H. C. Sio, and D. Macdonald, Applied Physics Letters **103**, 192112 (2013).

[6] S. P. Phang, H. C. Sio, and D. Macdonald, Progress in Photovoltaics: Research and Applications **24**, 1547 (2016).

[7] Y. Zhu, M. K. Juhl, T. Trupke, and Z. Hameiri, IEEE J. Photovoltaics **7**, 1087 (2017).

[8] W. Shockley and W. T. Read Jr., Physical Review **87**, 835 (1952).

[9] F. D. Heinz *et al.*, Journal of Applied Physics **118**, 105706 (2015).

[10] F. D. Heinz, L. E. Mundt, W. Warta, and M. C. Schubert, physica status solidi (RRL) – Rapid Research Letters **9**, 697 (2015).